Generalized scanning beam interference lithography system for patterning gratings with variable period progressions

G. S. Pati,[a] R. K. Heilmann, P. T. Konkola, C. Joo, C. G. Chen, E. Murphy, and M. L. Schattenburg

Space Nanotechnology Laboratory, Center for Space Research, Massachusetts Institute of Technology, Cambridge, Massachusetts 02139

(Received 28 May 2002; accepted 16 September 2002)

We demonstrate a versatile interference lithography system that can continuously vary the pattern period and orientation during fabrication of general periodic structures in one or two dimensions. Initial experimental results, using closed-loop beam steering control and double exposures on a stationary substrate, are obtained in order to illustrate its principle of operation. A fringe-locking scheme for phase control is also demonstrated including discussion of issues related to future system developments. © *2002 American Vacuum Society.* [DOI: 10.1116/1.1520563]

I. INTRODUCTION

Fabrication of high-fidelity general periodic (chirped or quasiperiodic) structures in one or two dimensions with a small period has been of significant interest for various applications, including patterned magnetic media storage,[1] chirped Bragg gratings for time-delay or spectral-filtering applications,[2] photonic band-gap waveguides and emitters,[3] flat panel displays,[4] and diffractive optical elements.[5] Over the years, interference lithography (IL) has been combined with multiple-beam[6] or multiple-exposure interferometry[7] to be extensively used as a fabrication technique for patterning various kinds of structures, such as dot and hexagonal arrays as well as three-dimensional structures for some of these applications. The scanning beam interference lithography[8] (SBIL) system, currently under development in our laboratory, is designed to pattern large-area linear gratings or grids with subnanometer phase distortion. However, the geometrical constraints associated with free-space beam alignment and overlap do not allow the SBIL system to be used in general patterning as discussed earlier.

In a recent effort, we developed the concept for a prototype system that generalizes the use of phase-locked scanning beams in a SBIL system for general patterning in one or two dimensions. Such a system can rapidly configure the interfering beams by employing steering mirrors in a finite-conjugate optical system. Therefore, unlike the SBIL system, but using a similar phase-control mechanism, this system can progressively change the pattern period (or pitch) and orientation in a desirable fashion during large-area patterning on a continuously scanned substrate. When used in conjunction with multiple exposures, the system also eliminates the stringent substrate alignment requirement by replacing substrate rotation with physical rotation of the beams. Such a system is designated as a variable-period scanning beam interference lithography (VP-SBIL) system. The system has all the required degrees of freedom to be used as a fabrication tool for the various applications mentioned previously.

This article describes the design and development of an experimental VP-SBIL system. Dual-axis picomotor-driven gimbal mirrors are used under closed-loop control for continuously changing the pattern period and orientation. Experimental results for double exposures on a stationary substrate are presented in order to demonstrate the general patterning ability of the system. We also describe an elegant approach for phase control in the VP-SBIL system for large-area patterning. Finally, we discuss some of the issues related to the future system development.

II. SYSTEM DESCRIPTION

A schematic of the VP-SBIL system is shown in Fig. 1. An incoming beam from an Ar^+–laser ($\lambda = 351$ nm) is incident on a grating and the diffracted beams are input into a beam-steering system[9] that maintains beam stability necessary for interferometric patterning in a VP-SBIL system. The stable zero-order beam contains 98% of the input beam power and is approximately 2 mm in diameter with a Gaussian beam (TEM_{00} mode) intensity profile. The beam is spatially filtered and collimated to generate a beam (diameter ≈ 8 mm) with a relatively smooth intensity profile.

In order to generate the interfering beams for the VP-SBIL system, the zero-order beam is split energy efficiently into first diffracted orders of a phase grating (diffraction angle$= 5°$ and efficiency$= 0.3$). The propagating first-order diffracted beams from the grating, after reflection from a series of mirrors, are incident on two gimbal mirrors as shown in Fig. 1. These mirrors are mounted with dual-axis picomotors for steering the interfering beams and are precisely positioned on the object-side conjugate planes of a finite-conjugate optical system. A half-coated dielectric wedge-angle beam splitter is used to fold one of the interfering beam paths around the optical axis *Z*, creating a replica of the object-side conjugate plane accessible to one of the gimbal mirrors.

The beams, after deflection from the gimbal mirrors, pass through an optical system consisting of two singlet lenses arranged in a 4-f optical configuration and interfere in the back focal plane of the second objective lens, where the substrate is positioned. Beam deflection points on the mirrors

[a]Electronic mail: pati@snl.mit.edu

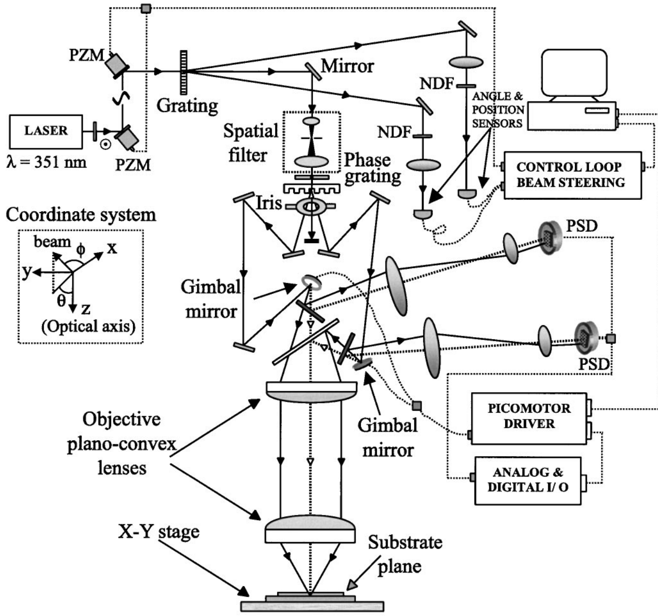

FIG. 1. Experimental diagram for the VP-SBIL system.

being conjugate to beam overlap on the substrate, the gimbal mirrors can steer the angle and orientation of the beams in order to continuously vary the pattern period and orientation, without changing the position of beam overlap on the substrate. Gimbal mirrors also produce beam deflection without on-axis translation, which is an essential feature.

Since the optical paths traversed by beams and their interference on the substrate are analogous to on-axis image formation in the optical system, spherical aberration associated with the lens system governs the extent of beam overlap in the transverse substrate plane *XY*. It causes the position of maximum beam overlap to vary along *Z* while changing the beam angle over the lens aperture. The effect is particularly pronounced while using a long focal length (i.e., long-working distance), and high numerical aperture (NA) (i.e., large-field angle) singlet lenses, as in the VP-SBIL system. To minimize this effect, a pair of infinite-conjugate singlet "best form" planoconvex lenses[10] (NA=0.11, 0.23 and $f=216$, 108 mm) are chosen and arranged in the 4-f optical configuration with their curved surfaces facing each other and the conjugate-ratio equal to the focal ratio of the lenses. The spot size of the image or beam overlap on the substrate (≈4.0 mm) is determined by the magnification (focal ratio, $M=f_2/f_1$) associated with the lens system. In Sec. II A, we present a simple quantitative analysis to estimate the effect of lens spherical aberration on beam overlap in the VP-SBIL system.

To precisely control beam angles and orientations, we used two identical optical beam alignment systems for the left and right interfering beams shown in Fig. 1. Using partially reflecting wedge-angle windows, the optical axes of the two subsystems are aligned with the optical axis of the VP-SBIL lens system described earlier. These subsystems use a combination of imaging lens ($f_i=200$ mm) and Fourier lens ($f_f=50$ mm) to transform the beam angle θ (measured with respect to the Z axis) into displacement. Position sensing detectors (PSDs) (4×4 mm^2, position nonlinearity$<0.3\%$) along with National Instrument 16 bit analog DAQ control hardware are used at the back end of the beam alignment systems to measure beam positions with a resolution of approximately 0.24 μm.

Choosing appropriate magnification (M_i) during imaging, allows us to contain the beam displacement $d=1/M_i \times f_f \tan\theta$ on the PSDs to within their physical dimensions for the entire range of beam angles, i.e., from 0° to 14° (NA limited). Position readings obtained from the PSDs are then calibrated in terms of beam angles by steering the left and right interfering beams over the whole field of the lens aperture. For a desirable pattern period and orientation, the control algorithm uses a linear fit to the calibration data to determine the final beam positions on the PSDs and uses the control hardware (NI 6503 for 5V TTL I/O signals) to drive the picomotors, thereby steering the beams from their current position to the final position. In this process, the control loop sequentially drives six picomotors on gimbal mirrors in a closed-loop operation to continuously vary the beam angle θ from 0° to 14° and beam orientation over the half space (i.e., $\phi=-90°-90°$). This corresponds to variation in grating period Λ from being as large as the spot diameter (≈4 mm) to a smallest period of about 800 nm. Although very fine displacement of the picomotors (30 nm/step) can provide high angular resolution (≈2 μrad) in beam steering and hence, pattern period and orientation control in VP-SBIL, currently the resolution is limited to ≈0.015 mrad by system magnification M_i and the position resolution and physical size of PSDs.

Figure 2 depicts the effect of spherical aberration on beam overlap at the back focal plane of the second objective lens in a VP-SBIL system, for small (paraxial, $\sin\theta\sim\theta$) and large (marginal) beam angles. The longitudinal extents (or depth of foci) are given by

$$L_{zp}=\frac{\omega_o}{\sin\theta_p},\quad L_{zm}=\frac{\omega_o}{\sin\theta_m},\tag{1}$$

where ω_o is the Gaussian beam waist and θ_p, θ_m represent the half angles of the paraxial and marginal beams with respect to optical axis, respectively. Since $\theta_m>\theta_p$, L_{zm} is smaller than L_{zp} and $(L_{zm})_{min}=\omega_o$ corresponds to the depth of focus for NA=1. The distance between the planes where the paraxial and marginal beams have maximum transverse overlap is a measure of longitudinal spherical aberration (LSA). The presence of spherical aberration will separate the maximum transverse beam-overlap planes and cause the beam overlap to vary on the substrate plane with the angle of the beams. To mitigate such an effect and ensure an extended beam overlap on the substrate plane over a range of beam angles, it is necessary that LSA$\ll L_{zm}$.

If the substrate is positioned in the plane where marginal beams have the maximum overlap, the transverse extent of overlap for the paraxial beams in this plane is given by

$$T'_p=(L_{zp}-2\text{LSA})\tan\theta_p.\tag{2}$$

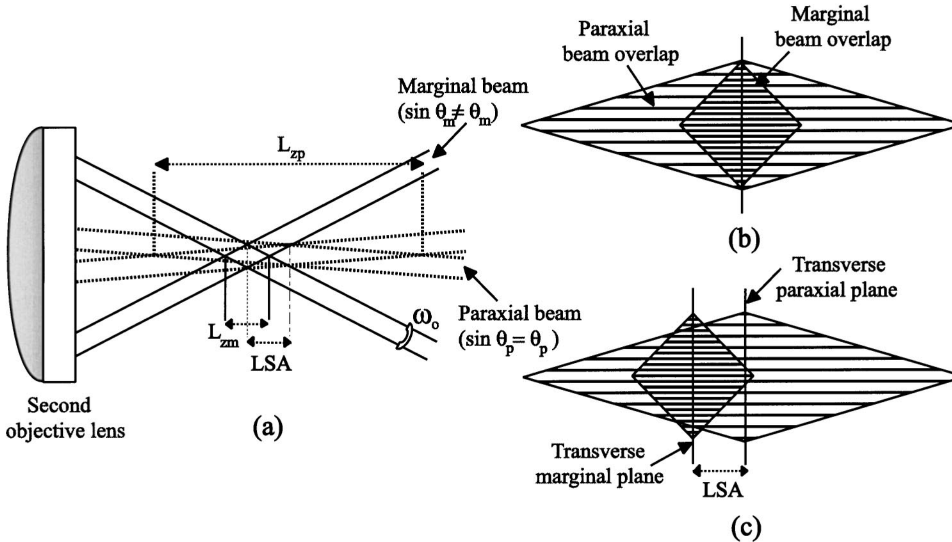

FIG. 2. (a) Effect of lens spherical aberration on beam overlap. Marginal and paraxial beam-overlap regions with superposed grating images (b) without spherical aberration and (c) with spherical aberration.

This corresponds to a fraction α of transverse marginal beam overlap T_m, that is given by

$$\alpha=\frac{T_p'}{T_m}=\frac{(L_{zp}-2\text{LSA})}{\omega_o}\tan\theta_p\cos\theta_m. \quad (3)$$

In order to estimate the magnitude of spherical aberration in VP-SBIL lens system, we used an approximate expression[10] for third-order longitudinal spherical aberration for a singlet lens:

$$\text{LSA}=\frac{kf}{f/\#^2}, \quad (4)$$

where k is the aberration coefficient and $f/\#$ is the f number of the lens. For a "best form" singlet planoconvex lens, the value of the aberration coefficient k is 0.272. For two planoconvex lenses used in the VP-SBIL system, the total spherical aberration contribution is approximately given by the sum of the individual lens aberrations. Using appropriate lens parameters, we obtain the magnitude of LSA for the VP-SBIL system to be ~9 mm, which is well below the marginal depth of focus L_{zm}, i.e., 16.5 mm. This was also verified using ray tracing with Code V software. Fractional beam overlap α is estimated to be close to 90%. The rest of the area where the paraxial beams do not overlap contributes to a dc bias and loss in grating contrast that are detrimental to large-area patterning. However, such a feature of the VP-SBIL system can be significantly improved either by using aberration balanced lens design or using aspheric lenses.

III. EXPERIMENTAL RESULTS AND DISCUSSIONS

We performed experiments in a VP-SBIL system using double exposures on a stationary substrate. Closed-loop beam alignment systems are used to steer the beams between the exposures in order to create various kinds of two-dimensional (2D) periodic structures. A grating image during the second exposure is registered precisely on top of the first image to submicron accuracy, which is not generally practicable with a rotating substrate. The present approach has also the ability to vary the pattern period between the exposures.

Short exposure (0.01 s) schedules are chosen for these experiments in order to maintain good image contrast in the absence of phase-control in a VP-SBIL system. Positive photoresist (Shipley 1830) spin coated on Si substrate (1-μm thickness) is used in patterning. During each exposure, the resist is exposed to approximately an energy density (or dose) of 50 mJ/cm^2 and subsequently developed using Microposit developer for 45 s. The double-exposure experiment takes advantage of the wide process latitude of the photoresist.

Figure 3(a) shows a scanning electron microscopy (SEM) micrograph of a double exposure result from the sample. The pattern shows a periodic square array generated by rotating the interference pattern by 90° between exposures. For a certain exposure time, the region where the intensity maxima of the two patterns overlap receives a clearing dose. From these regions, the resist completely dissolves after developing, forming an array of holes that clearly appear in the resist layer shown in Fig. 3(a). "Post"-like structures are also formed in the regions where the minima of the two patterns overlap. Intermediate intensity regions corresponding to overlap of maxima and minima of the patterns form "saddle points." We also see standing wave patterns around each post because of strong reflection from the substrate/resist interface which is not antireflection coated. Figure 3(b) shows a microscope image of the same structure over a large sample area $(100\times 100\ \mu\text{m}^2)$. This shows that pattern uniformity varies over a large area due to dose variation resulting from beam intensity nonuniformity. However, this can be taken care of by tightly overlapping adjacent scans during large-area patterning in VP-SBIL, using precise and controlled substrate scanning.

Figure 3(c) shows a microscope image for double exposure to form a hexagonal array, when the beams are rotated by 60° between exposures. This pattern does not have a complete hexagonal symmetry, as true symmetry would require a

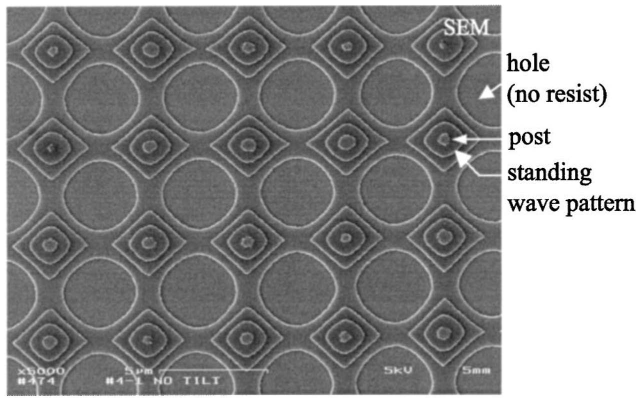

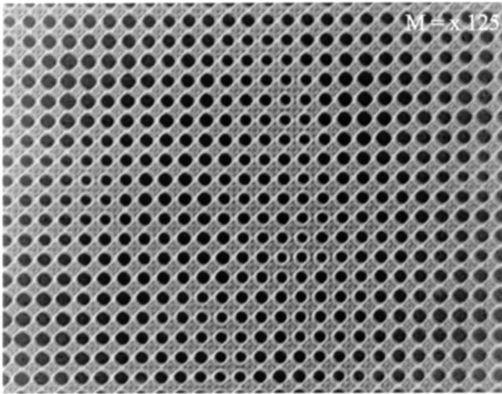

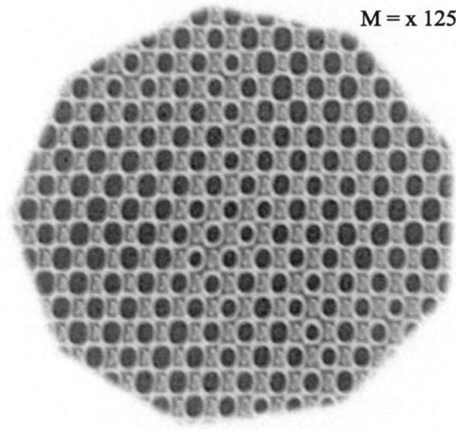

FIG. 3. Double-exposure results: (a) SEM micrograph, (b) microscope image of square periodic array with average pattern periodicity $\Lambda = 4.8\ \mu$m and hole diameter $D = 2.4\ \mu$m; (c) microscope image of a hexagonal array with average pattern periodicity $\Lambda = 7.2\ \mu$m and hole diameter $D = 3.6\ \mu$m.

third exposure (further 60° rotation of the beams) that exactly registers on the previous two. However, this is difficult to ensure in a VP-SBIL system without active phase control. On the other hand, resist nonlinearity renders some additional Fourier components that make the double-exposure patterns look like the hexagonal array. Again, the pattern nonuniformity is attributed to the dose variation across the beam overlap. Our future work will explore pattern reproducibility, distortions, uniformity, and yield of multiple exposure techniques in VP-SBIL for various applications.

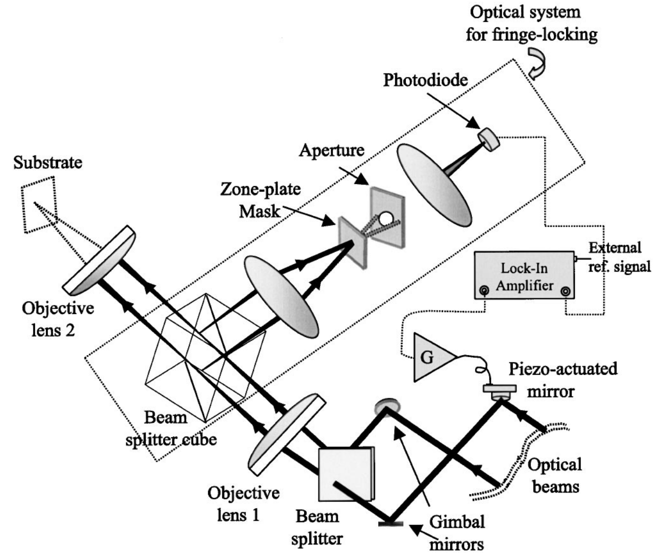

FIG. 4. Homodyne fringe-locking scheme using a Fresnel zone-plate in VP-SBIL system.

IV. PRINCIPLE OF INTERFEROMETRIC PHASE CONTROL IN VP-SBIL

Environmental perturbations induced by vibrations, turbulence, thermal drift, and pressure gradients cause phase drift between the interfering beams in any IL system including the VP-SBIL system. This results in motion of the interference pattern leading to image contrast degradation. It is possible to compensate for fringe motion by detecting the phase drift using interferometric (homodyne or heterodyne) schemes, and then actuating a phase modulating device in an error-driven feedback loop to compensate for the phase drift.[12] In the VP-SBIL system, where the beam paths continuously evolve, we devised a scheme using a zone plate to obtain an interferometric Moiré signal for phase control or fringe locking.

Figure 4 shows a homodyne fringe-locking scheme for the VP-SBIL system. A mask containing a zone plate is positioned at the point where the interfering beams overlap. The zone plate contains a wide range of spatial frequencies defined by the quadratically varying zone width across its spatial aperture. For a wide range of beam angles and arbitrary beam rotation, spatial frequencies of the interference pattern, i.e., $(\sin \theta/\lambda)$, closely match with spatial frequencies in the zone plate. This produces near collinearly copropagating diffracted fields from incident beams, that coherently superpose to form interferometric Moiré zones in the far field centered on the optical axis. A comprehensive analysis on the origin of Moiré zones and their use in precision fringe metrology are discussed by Joo *et al.*[11] Figures 5(a) and 5(b) show computed Moiré patterns for relative phase shifts 0 and π between the beams, which suggests that the Moiré pattern can be sampled over a small area and the optical power can be integrated using a lens (as shown in Fig. 4) onto a detector to produce a phase-sensitive signal for fringe locking.

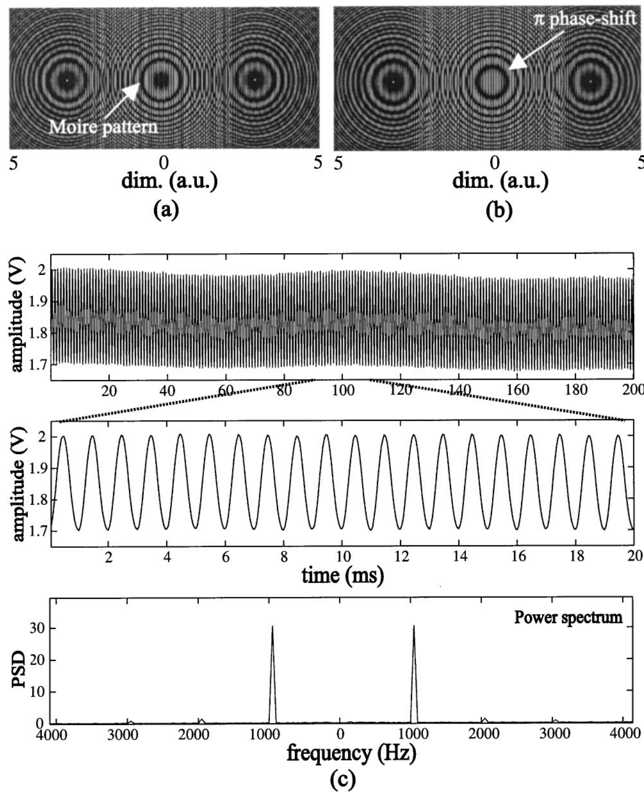

FIG. 5. Computed far-field Moiré patterns for (a) zero and (b) π phase shift between interfering beams. (c) Experimental result for phase-sensitive interferometric Moiré signal.

The zone plate that is currently available to us has an extremely low-light throughput at the source wavelength (351 nm), and the range of spatial frequencies possessed by it favors large-angle interference. We therefore set up an experiment using a He–Ne laser ($\lambda = 632.8$ nm) with a beam angle of 41° to demonstrate the principle of fringe locking. Figure 5(c) shows the experimental result for a sampled Moiré signal (with its power spectrum) received from the photodiode when the phase of one of the interfering beams is sinusoidally modulated at a frequency of 1 kHz. Such a signal can be used in fringe locking. For higher fringe-locking performance, this scheme can be easily extended to digital heterodyne fringe locking by introducing frequency modulation.[12]

One of our future goals is to develop the VP-SBIL system for rapid patterning of low-distortion chirped gratings and other quasiperiodic structures over a large area. This would require us to use interferometrically controlled stage motion and accurate heterodyne fringe control in the VP-SBIL system. Due to the very nature of a frictional drive in the picomotors currently used in the VP-SBIL system, we currently experience displacement jitter and low-bandwidth operation under feedback control. The picomotors will be subsequently replaced by voice coil-actuated fast steering mirrors that can offer similar submicroradian angular adjustability as picomotors and perform closed-loop operation at frequencies >1 kHz. Optimized aberration-balanced design would be considered to increase the NA limit and system magnification for the VP-SBIL system.

V. CONCLUSIONS

In summary, we demonstrated the concept of an interference lithography system with a general patterning ability and discussed a fringe-locking scheme for phase control in the system that can enable high-uniformity and low-distortion patterning for our future applications. Issues related to lens aberration and device properties are also discussed in the context of future system development.

ACKNOWLEDGMENTS

The authors gratefully acknowledge the assistance of Robert Fleming from MIT Space Nanotechnology Laboratory and support from DARPA under Grant No. DAAG55-98-1-0130 and NASA under Grant No. NAG5-5271.

[1] C. A. Ross, H. I. Smith, T. Savas, M. L. Schattenburg, M. Farhoud, M. Hwang, M. Walsh, M. C. Abraham, and R. J. Ram, J. Vac. Sci. Technol. B **17**, 3168 (1999).
[2] Q. Zhang, D. A. Brown, L. J. Reinhart, and T. F. Morse, Opt. Lett. **20**, 1122 (1995).
[3] D. Cassagn, C. Jouanin, and D. Bertho, Phys. Rev. B **53**, 7134 (1996).
[4] C. O. Bozler, C. T. Harris, S. Rabe, D. D. Rathman, M. A. Hollis, and H. I. Smith, J. Vac. Sci. Technol. B **12**, 629 (1994).
[5] M. C. Hutley, J. Mod. Opt. **37**, 253 (1990).
[6] V. Berger, O. Gauthier-Lafaye, and E. Costard, Electron. Lett. **33**, 425 (1997).
[7] S. H. Zaidi and S. R. J. Brueck, J. Vac. Sci. Technol. B **11**, 658 (1993).
[8] C. G. Chen, P. T. Konkola, R. K. Heilmann, G. S. Pati, and M. L. Schattenburg, J. Vac. Sci. Technol. B **19**, 2335 (2001).
[9] P. T. Konkola, C. G. Chen, R. K. Heilmann, and M. L. Schattenburg, J. Vac. Sci. Technol. B **18**, 3282 (2000).
[10] W. J. Smith, *Modern Optical Engineering* (McGraw–Hill, Boston, MA, 1990).
[11] C. Joo, G. S. Pati, C. G. Chen, P. T. Konkola, R. K. Heilmann, and M. L. Schattenburg, J. Vac. Sci. Technol. B, these proceedings.
[12] R. K. Heilmann, P. T. Konkola, C. G. Chen, G. S. Pati, and M. L. Schattenburg, J. Vac. Sci. Technol. B **19**, 2342 (2001).